Published online June 28, 2004

3446–3455 *Nucleic Acids Research, 2004, Vol. 32, No. 11*
DOI: 10.1093/nar/gkh658

Thermodynamic and structural characterization of 2′-nitrogen-modified RNA duplexes

John W. Pham, Ishwar Radhakrishnan and Erik J. Sontheimer*

Department of Biochemistry, Molecular Biology and Cell Biology, Northwestern University, 2205 Tech Drive, Evanston, IL 60208-3500, USA

Received May 11, 2004; Revised and Accepted June 1, 2004

ABSTRACT

2′-aminonucleosides are commonly used as sites of post-synthetic chemical modification within nucleic acids. As part of a larger cross-linking strategy, we appended alkyl groups onto the N2′ position of 2′-amino-modified RNAs via 2′-ureido and 2′-amido linkages. We have characterized the thermodynamics of 2′-amino, 2′-alkylamido and 2′-alkylureido-modified RNA duplexes and show that 2′-ureido-modified RNAs are significantly more stable than analogous 2′-amido-modified RNAs. Using NMR spectroscopy and NMR-based molecular modeling of 2′-modified RNA duplexes, we examined the effects that 2′-nitrogen modifications have on RNA helices. Our data suggest that the 2′-ureido group forms a specific intra-nucleoside interaction that cannot occur within 2′-amido-modified helices. These results indicate that 2′-ureido modifications are superior to analogous 2′-amido ones for applications that require stable base pairing.

INTRODUCTION

Advances in nucleic acid chemistry have significantly enhanced our understanding of RNA structure, function and stability. It is now possible to modify RNAs on their bases, sugars and phosphate backbones to generate a variety of chemically useful derivatives. Many of these modifications can be achieved in both RNA and DNA, where they have been used successfully to study ribozyme catalysis (1–5), DNA repair (6), pre-messenger RNA splicing (7–9) and other cellular functions.

In recent years, the C2′ position of the ribose sugar has been a particular focus of interest, in part because C2′ modifications often enhance nuclease resistance (10–12). However, C2′ substituents can also destabilize RNA duplexes. C2′ modifications affect the preferred sugar puckering of both DNAs and RNAs, depending on the type of atom at the 2′-position (13,14). For example, 2′-*O*-modified oligonucleotides (and those modified with other electronegative atoms) favor the C3′-*endo* (N-type) conformation that is characteristic of RNA, explaining the stabilizing effect these modifications have in RNA and DNA/RNA duplexes (12). In contrast, heteroatom substitutions involving nitrogen, like 2′-amino and 2′-amido, push the equilibrium of ribonucleotides from the C3′-*endo* conformation toward a more DNA-like C2′-*endo* (S-type) conformation (15,16). Depending on the structural context, these shifts in sugar pucker can destabilize modified helices. Despite this caveat, the C2′ position is still a useful target because modifications at this site can be achieved post-synthetically; furthermore, unlike base modifications, C2′ modifications are not known to perturb base-pairing interactions.

We use 2′-modification chemistry to introduce dithiol-containing functional groups into RNA duplexes. These functional groups are part of a cross-linking strategy that we are developing to trap RNAs, rapidly and reversibly, in large ribonucleoprotein assemblies like the spliceosome. Our design, based on a technique for fluorescently labeling protein (17,18), relies on the high affinity of trivalent arsenic for sulfur. By engineering dithiols into opposite strands of complementary RNAs, it may be possible to trap transient RNA duplexes using an organic molecule bearing two trivalent arsenic atoms. We have modified RNA duplexes at their C2′ positions and have characterized how the modifications affect RNA stability. We show that 2′-ureido-modified RNA duplexes are significantly more stable than other nitrogen-containing derivatives, but are less stable than unmodified RNA duplexes. Finally, using NMR spectroscopy, we explore the structural consequences of introducing these modifications both to gain insight into the factors that influence duplex stability and to guide our cross-linking design.

MATERIALS AND METHODS

All compounds were obtained from Aldrich unless noted. Thin layer chromatography plates were purchased from Selecto Scientific. NMR spectra of small molecules were recorded on a 400 MHz Varian spectrometer. High-performance liquid chromatography (HPLC) was performed on a Hewlett Packard Series 1100 chromatography system and matrix-assisted laser desorption ionization time-of-flight (MALDI-TOF) analysis was performed on a Voyager DE-Pro spectrometer (PerSeptive Biosystems).

Synthesis

4-carboxy-1,2-dithiolane (Asparagusic acid), **(1)**, was synthesized in five steps from diethyl(bis-hydroxymethyl)malonate as described previously (19).

*To whom correspondence should be addressed. Tel: +1 847 467 6880; Fax: +1 847 491 2467; Email: erik@northwestern.edu

1,3-dithiobenzylacetone as well as compound *1,3-dithiobenzyl oxime* (see below) were synthesized by a modified method described by Kojima (20). Sodium metal (4.6 g) was suspended in a stirring solution of 300 ml anhydrous ethanol. After the mixture was cooled on ice, thiobenzyl alcohol (24.9 g, 0.23 mol) was added. A solution of dichloroacetone (12.15 g, 0.1 mol) (Fisher) in 150 ml of ethanol was slowly added over a period of 5 min, during which a white precipitate was formed. The mixture was stirred at room temperature for an additional 3 h. The solution was slowly rotary evaporated to avoid bumping and the remaining residue was dissolved in 150 ml water and extracted with ether (4×50 ml). The ether layer was washed with 50 ml water, dried over Na_2SO_4, and evaporated to give 1,3-dithiobenzylacetone as a yellow oil (29.4 g, 97.4%). ^{1}H NMR ($CDCl_3$) δ3.2 (4H, s), δ3.7 (4H, s), δ7.3 (10H, m).

1,3-dithiobenzyl oxime. A total of 24.2 g (0.08 mol) of 1,3-dithiobenzyl acetone and hydroxylamine hydrochloride (26.4 g, 0.38 mol) were dissolved in 200 ml of anhydrous ethanol. A total of 10 M NaOH (40.4 ml) was added to the mixture, which was then refluxed for 90 min. After cooling, water was added and the mixture was extracted with ether (3×50 ml). The ether layer was washed with water, dried over Na_2SO_4 and rotary evaporated. The remaining material was dissolved in dichloromethane (DCM) and chromatographed on a silica gel column with DCM as the mobile phase. Fractions were collected and the eluent monitored by thin layer chromatography with DCM as the mobile phase ($R_f = 0.31$). Product-containing fractions were pooled, evaporated and recrystallized from ethanol to give 1,3-dithiobenzyl oxime as needle-like white crystals (11.9 g, 46.7%). ^{1}H NMR ($CDCl_3$) δ3.2 (2H, s), δ3.5 (2H, s), δ3.62 (2H, s), δ3.73 (2H, s), δ7.25 (10H, m), δ7.3 (1H, s).

2-amino-1,3-bis(thiobenzyl)propane hydrochloride. A total of 8.0 g (25 mmol) of 1,3-dithiobenzyl oxime was dissolved in 50 ml of dry ether. Lithium aluminum hydride (2 g) was slowly added to the solution, which was stirred under nitrogen overnight. The mixture was cooled in an ice-water bath and 20 ml water was slowly added. It was then dried over Na_2SO_4 and rotary evaporated to give a yellow oil. ^{1}H NMR ($CDCl_3$) δ1.8 (2H, s), δ2.3 (2H, dd), δ2.9 (1H, m), δ3.7 (4H, s), δ7.3 (10H, m). A total of 80 ml of 10% HCl was added and mixed with the oil by pipetting. After 10 min, a yellowish-white precipitate was formed. The precipitate was filtered, washed with ether and recrystallized from ethanol (seeding with crude precipitate was required) to give the amine hydrochloride as a needle-like crystal (1.85 g, 22%).

4-amino-1,2-dithiolane. Gaseous ammonia (~100 ml) was condensed in a dry ice/acetone bath. A total of 1.7 g (5 mmol) of 2-amino-1,3-bis(thiobenzyl)propane hydrochloride (dissolved in 15 ml of ether) was added to the stirring, condensed ammonia. Sodium metal (0.9 g) was then added to the mixture and stirred for 25 min. To destroy the excess sodium metal 10 ml of ethanol was slowly added. The mixture was then removed from the dry ice/acetone bath and allowed to warm to room temperature, dispersing the ammonia. A total of 200 ml of water was then added and the solution was acidified with HCl. Some crystals formed, which were removed by filtration. The deprotected thiols were then oxidized and isolated as described previously (21) to give a yellow powder (0.41 g, 52%). ^{1}H NMR (D_2O) δ3.2 (4H, d of m), δ4.35 (1H, m).

4-isocyanato-1,2-dithiolane, **(2)**. The isocyanate was prepared from 4-amino-1,2-dithiolane with diphosgene using a previously described protocol for converting aliphatic amines into isocyanates (22).

RNA modification

For the experiment shown in Figure 1, the two complementary oligoribonucleotides, 5′-AGCAAA(2′-NH_2U)GACA-3′ and 5′-UGUCA(2′-NH_2U)UUGCU-3′, were synthesized (Dharmacon), deprotected and purified by reverse phase HPLC. For coupling to asparagusic acid **(1)**, 6 nmol of each RNA was reacted with 40 mM of the acid, and 25 mM of 1-[3-(dimethylamino)propyl]-3-ethylcarbodiimide hydrochloride (DEC), in 180 mM of MES–NaOH, pH 6.5 (500 µl total reaction volume) at 37°C. After 1 h, an additional equivalent of acid and DEC were added and the reaction was incubated at 37°C for 1 h. The organic contaminants in the mixture were extracted with butanol and the RNA was HPLC purified and analyzed by MALDI-TOF mass spectrometry (MS). For coupling with 4-isocyanato-1,2-dithiolane

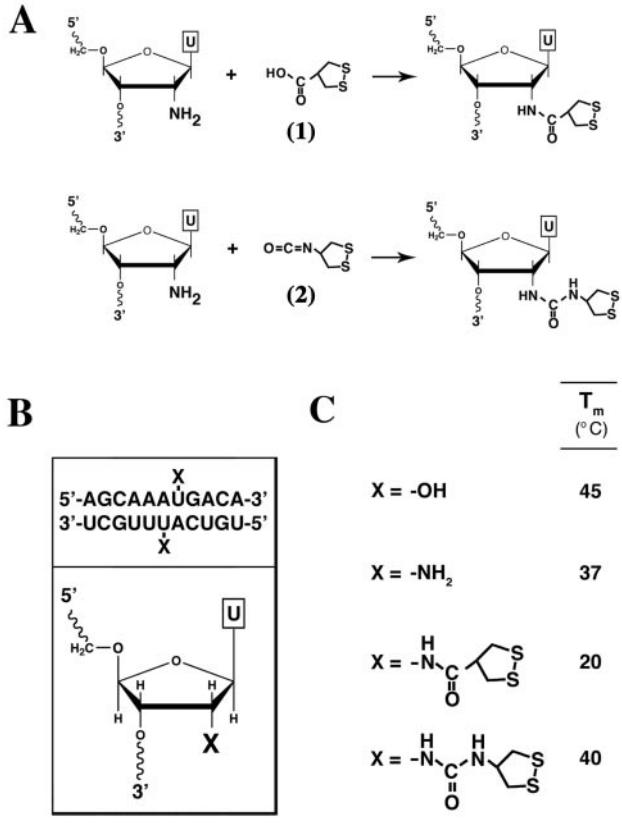

Figure 1. Preparation and melting analysis of RNAs with 2′-dithiolane modifications. (**A**) RNAs bearing single 2′-amino modifications were derivatized with asparagusic acid, **1**, or 4-isocyanato-1,2-dithiolane, **2**, to give 2′-dithiolane-modified RNAs via amido or ureido linkages, respectively. (**B**) When the modified, non-self-complementary, 11mer RNAs are annealed, the 2′-modified groups (labeled 'X') are on opposite strands of the double helix, displaced by 1 bp. For reference, the C2′ position of the RNA sugar is shown in the bottom panel. (**C**) The melting temperature of each duplex (shown in B) was determined by measuring the inflection point of the melting curve. The C2′ substituent, shown on the left, corresponds to 'X' from (B). Melting temperatures of RNAs where X = 2′-OH and 2′-NH_2 were also determined and are shown for comparison.

(2), the oligos were treated as described previously (23). Each product was purified by reverse phase HPLC using an Ultrasphere ODS C-18 column (Beckman) and analyzed by MALDI-TOF MS.

For the thermodynamic analysis in Figure 2 and for all NMR experiments, a self-complementary oligoribonucleotide (chosen to simplify NMR analysis), 5′-CGCAA(2′-NH_2U) UGCG-3′, was synthesized (Dharmacon), deprotected and HPLC purified. A total of 6 nmol of the RNA were coupled with propionic acid (to form 2′-amido RNA), using DEC as described above. For coupling with ethyl isocyanate, the oligo was treated as described previously (23). Each product was purified by anion exchange HPLC using a DNAPac PA-100 semi-prep column (Dionex) and verified by MALDI-TOF MS. For melting analysis, modified oligos were desalted by gravity chromatography on a Sephadex G-10 column (15 ml bed volume; Amersham). For NMR analysis, oligos were additionally subjected to counter-ion replacement by gravity chromatography on a DOWEX 50WX8-100 column (15 ml bed volume; Aldrich) that was pre-charged with Na^+ and rinsed extensively with water.

Melting analysis

For the experiments shown in Figure 1, RNA samples were suspended in buffer (0.5 μM in 140 mM NaCl, 10 mM PIPES, pH 7.0) and annealed by heat treating (95°C, 2 min) and slow cooling to room temperature. Melting data were collected at A_{260} in triplicate in a double-beam UV-Vis-NIR spectrophotometer (Cary 500, Varian) from 5 to 85°C at a rate of 0.5°C/min. T_m values were determined by calculating the inflection point of the melting curve (Cary UVwin v. 2.0).

For the experiments shown in Figure 2, RNA samples were suspended in buffer (6 or 45 μM in 1 M NaCl, 10 mM PIPES, pH 7.0, 0.5 mM EDTA), annealed and analyzed as described above (except that the absorbance of the 45 μM samples were measured at A_{280} rather than A_{260}). T_m values were calculated from a plot of α versus T (the fraction of duplex at temperature, T). Values for ΔH° and ΔS° were calculated as described previously (24) and used to determine ΔG°_{37}.

NMR analysis

Purified, desalted and freeze-dried oligoribonucleotides were suspended in a buffer containing 10 mM sodium phosphate, pH 6.8 and 1 mM EDTA. They were annealed by incubation at 95°C for 2 min followed by slow cooling to room temperature (duplex concentration ~0.5 mM). For these experiments, RNA duplexes containing 2′-OH, 2′-amino and 2′-ethylureido substituents on the U6 residue were analyzed.

All NMR spectra of RNA samples were recorded on a 600 MHz Varian Inova spectrometer and processed using FELIX (Accelrys, Inc.). One-dimensional (1D) ^{1}H NMR experiments were performed in H_2O/D_2O (90% to 10%) at 10° increments from 5 to 45°C. Two-dimensional ^{1}H–^{1}H nuclear Overhauser effect spectra (NOESY) were recorded at 15°C (75 and 200 ms mixing times). Two-dimensional homonuclear double quantum filtered correlation spectra

A

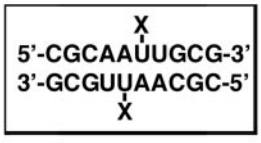

B

	6 μM duplex RNA				45 μM duplex RNA			
	ΔG°_{37} (kcal/mol)*	ΔH° (kcal/mol)*	ΔS° (cal/mol*K)*	T_m (°C)	ΔG°_{37} (kcal/mol)*	ΔH° (kcal/mol)*	ΔS° (cal/mol*K)*	T_m (°C)
X = 2′-OH	-12.25	-76.0	-206.9	58.2	-13.72	-92.4	-253.6	64.6
X = 2′-NH_2	-9.82	-59.9	-161.6	50.0	-10.61	-74.2	-205.1	56.6
X = 2′-NH-C(=O)-Et	—	—	—	—	-8.39	-50.2	-134.8	51.1
X = 2′-NH-C(=O)-NH-Et	-10.84	-70.5	-192.3	53.0	-12.02	-83.0	-228.7	60.5

Figure 2. Thermodynamic analysis of 2′-amido and 2′-ureido RNAs. (**A**) A self-complementary 10mer RNA was designed that places the 2′-modified groups (labeled 'X') across the minor groove from one another (as in Figure 1). A self-complementary duplex (rather than the non-self-complementary one used in Figure 1) was chosen to simplify subsequent NMR analyses. (**B**) Thermodynamic parameters were extracted from equilibrium melting curves (performed in triplicate) measured at 6 or 45 μM duplex RNA concentrations (in 1 M NaCl). Dashes indicate that thermodynamic parameters could not be determined due to an anomalous melting profile. Thermodynamic parameters of RNAs where X = 2′-OH and 2′-NH_2 are shown for comparison. Asterisks denote the estimates of standard errors for ΔG°_{37}, ΔH°, and ΔS° (5, 7 and 9% respectively) (37,38).

(DQF-COSY) and total correlation spectra (TOCSY) were also recorded at this temperature. H1′ and all base protons were unambiguously assigned by tracing the intra- and inter-residue connections from the H1′/H5-to-base region of the NOESY spectra. H2′ and H3′ protons were distinguished from one another by NOEs with intra- and inter-residue base protons (particularly H5 and H6 of pyrimidines). These assignments were supported by data from COSY and TOCSY spectra. Many H4′ and H5′/H5″ protons were more difficult to distinguish and, therefore, not assigned.

Molecular modeling

The volumes of all unambiguously assigned NOESY cross peaks from 75 ms mixing time experiments were measured and used as distance inputs in molecular modeling calculations. Inter-proton distances were estimated by using the averaged volume of all non-terminal H5-H6 cross peaks as reference (distance = 2.5 Å). Structure calculations were conducted with CNS (25) using A-form RNA duplexes as starting models. Coordinates for the unmodified or appropriately modified starting model duplexes were generated using InsightII (Accelrys, Inc.). Simulated annealing was achieved by heating the molecule to 1000 K in 5 ps and cooling to 0 K in 15 ps (stepsize = 1 fs). The resulting structures were subjected to 500 steps of energy minimization. Electrostatic terms were included in the potential energy function during this minimization. Counter-ion and solvent effects were mimicked by using a distance-dependent dielectric function and by reducing the charge on the phosphate groups (26). A number of additional restraints were employed in the structure calculations. These include hydrogen bonding distance restraints since NOEs characteristic of Watson-Crick base pairs could be detected in 2D NOESY spectra recorded in H_2O. Base pair planarity constraints were introduced to reduce propeller twisting. Backbone torsion angles were broadly restrained to ranges found in A- and B-form helices as described previously (27). Since DQF-COSY and TOCSY experiments did not reveal patterns characteristic of S-type sugar conformations for any of the samples, the riboses were constrained to N-type conformation ($\nu_0 = 0° \pm 12°$, $\nu_2 = 36° \pm 4°$). Because of the self-complementary nature of the RNA duplexes, a non-crystallographic 2-fold axis of symmetry was enforced. For the 2′-ethylureido RNA, the structure was additionally constrained to each of the four possible dihedral angle combinations for the ureido group, assuming planarity. All configurations, save one, resulted in several large NOE violations (>1 Å). Since NMR data were most consistent with this one conformation, we constrained the dihedral angles of the ureido group to reflect the data. A total of 10 structural models were generated for each input RNA. These 10 structures were, in turn, used as inputs for a second round of calculations using an identical simulated annealing-energy minimization protocol. Model images were generated using GRASP (28) and Rasmol (29).

RESULTS

We aim to develop a technique for rapid, specific and reversible RNA cross-linking. To achieve this goal, we first synthesized and attached dithiolane groups onto single-stranded, complementary, 11mer RNAs bearing single 2′-aminouridine substitutions. The dithiolanes were attached to the 2′-aminouridines in two ways using previously described chemical approaches (30,31): via a carboxylic acid, **1**, to generate a 2′-amido-linked dithiolane (Figure 1A, top) or via an isocyanate, **2**, to generate a 2′-ureido-linked dithiolane (Figure 1A, bottom). When annealed, the RNAs form a model duplex that positions the 2′-dithiolane groups on opposite strands of the double helix, displaced by a single base pair in the 5′ direction (relative to the top strand of the duplex) (Figure 1B). Since the dithiolanes are attached at the C2′ position, they are situated in the minor groove of the annealed RNA helix. After annealing, they can be reduced to give 2′-dithiol moieties that, in principle, can bind an exogenous, thiophilic cross-linking molecule.

We assessed the stability of the modified RNA duplexes because, for optimal activity, the 2′-dithiols should not significantly perturb the RNA helix. Therefore, we measured the melting temperature (T_m) using a UV-Vis-NIR spectrophotometer. For comparison, we also tested 2′-hydroxyl and 2′-amino RNA duplexes. The 2′-hydroxyl RNA was most stable ($T_m = 45°C$) (Figure 1C). The 2′-ureido modification was only mildly destabilizing ($T_m = 40°C$) and was, in fact, less destabilizing than the 2′-amino modification ($T_m = 37°C$). Interestingly, the 2′-amido-modified RNA duplex was very unstable ($T_m = 20°C$), even though it resembles the 2′-ureido RNA in its atomic structure (Figure 1C).

To understand better the destabilizing effect of the 2′-amido modification, we performed a more rigorous thermodynamic analysis using RNAs modified with commercially available reagents. These reagents, propionic acid and ethyl isocyanate, react with 2′-amino groups to yield 2′-ethylamido- and 2′-ethylureido-modified RNAs, respectively. For these experiments, we analyzed the thermal melting of a self-complementary 10mer RNA duplex (Figure 2A). For comparison, 2′-hydroxyl- and 2′-amino-modified RNAs were also tested. At low salt concentrations, the melting profiles of the 2′-amino and 2′-amido RNA samples were not sigmoidal, indicating that they contained contaminating hairpin structures (data not shown). To remedy this, we increased both the salt concentration (from 140 mM to 1 M NaCl) and the RNA concentration (from 0.5 to 6 μM duplex RNA). These conditions blocked hairpin formation in the 2′-amino RNA sample, but did little to prevent hairpin formation with the 2′-amido-modified RNA. As a result, it was not possible to extract thermodynamic information from this sample (Figure 2B, left). Hairpin contamination in the 2′-amido sample was eliminated only after increasing the RNA concentration to 45 μM (Figure 2B, right).

The thermodynamic data from the melting experiments again show that the 2′-amido modification is most destabilizing (Figure 2B, right). They indicate further that the destabilization of the 2′-amido-modified RNA duplex is caused by a significant loss of favorable enthalpy (Figure 2B, right). There is a large, simultaneous increase in favorable entropy, perhaps due in part to the disruption of ordered water molecules that line the minor groove of the RNA duplex (32). This increase in entropy, however, is not sufficient to overcome the enthalpic contribution to the free energy. Based on these results, we conclude that 2′-amido-modified RNA duplexes are not optimal cross-linking targets.

In contrast to the 2′-amido RNA, the energetic cost of the 2′-ureido modification is very modest. Again, there is a loss of favorable enthalpy, but it is relatively small, as is the gain in entropy (Figure 2B, right). Since the only difference between the ureido linkage and the amide linkage is the presence of the additional -NH- group, we hypothesized that this group may form stabilizing hydrogen bonding interactions at the minor groove edge. These hydrogen bonds would explain the increase in enthalpy, relative to the 2′-amido RNA. They may also constrain the 2′-ureido group, possibly minimizing the disruption of water molecules that hydrate the minor groove. This may explain the decrease in entropy of the 2′-ureido RNA relative to the 2′-amido duplex.

To examine this possibility further, we performed structural analyses of the 2′-ethylureido RNA duplex using NMR spectroscopy. 2′-hydroxyl and 2′-amino RNAs (identical to those used in Figure 2) were also tested for comparison. For each duplex, we first assessed Watson–Crick bonding interactions by examining the 1D proton NMR spectra in H_2O. The presence of resonances between 12 and 15 ppm, characteristic of hydrogen-bonded imino protons, confirmed the presence of Watson–Crick interactions. We monitored the changes in the imino proton region of 1D proton NMR spectra acquired at 10° increments from 5 to 45°C (Figure 3). At low temperatures (5–15°C), the resonances from all imino protons of all three RNAs were observed, including those of the 2′-modified U6 and terminal G10 residues (Figure 3). The presence of these proton peaks, particularly those of the central base pairs (U6 and U7, paired with A5 and A4, respectively), indicates that all three RNAs favor duplex over hairpin formation under these conditions (0.5 mM RNA in 10 mM sodium phosphate, pH 6.8 and 1 mM EDTA). At increased temperatures, the U6 and U7 imino resonances of the 2′-hydroxyl and 2′-ureido RNAs remain intact (Figure 3A and C). In contrast, those of the 2′-amino RNA progressively broaden and decrease in intensity, virtually vanishing at 45°C (Figure 3B). The instability caused by the 2′-amino modification has secondary effects on neighboring base pairs, since the G8 imino resonance is significantly diminished when compared with the corresponding residue on the 2′-hydroxyl or 2′-ureido RNAs. These results are consistent with our thermodynamic data showing that the 2′-amino-modified RNA duplex is less stable than both 2′-hydroxyl and 2′-ureido RNAs (Figure 2). Furthermore, the data show that the instability caused by the 2′-amino modification is localized to the central region of the RNA duplex in the vicinity of the modification.

We next performed 2D NOESY experiments, both to examine the geometry/positioning of the 2′-ureido group in solution and to determine whether it interacts with atoms in the minor groove of the duplex. As before, 2′-hydroxyl and 2′-amino RNAs were also examined. The volumes of all assigned NOESY cross peaks were measured, converted into approximate distances, and used as inputs for subsequent molecular modeling calculations.

Figure 4 shows NMR spectra of the 2′-ureido RNA from experiments in H_2O (Figure 4A) and D_2O (Figure 4B) that were collected at 15°C. The data from the experiment in H_2O again show that the hydrogen bonding interactions of the imino protons are intact (Figure 4A).

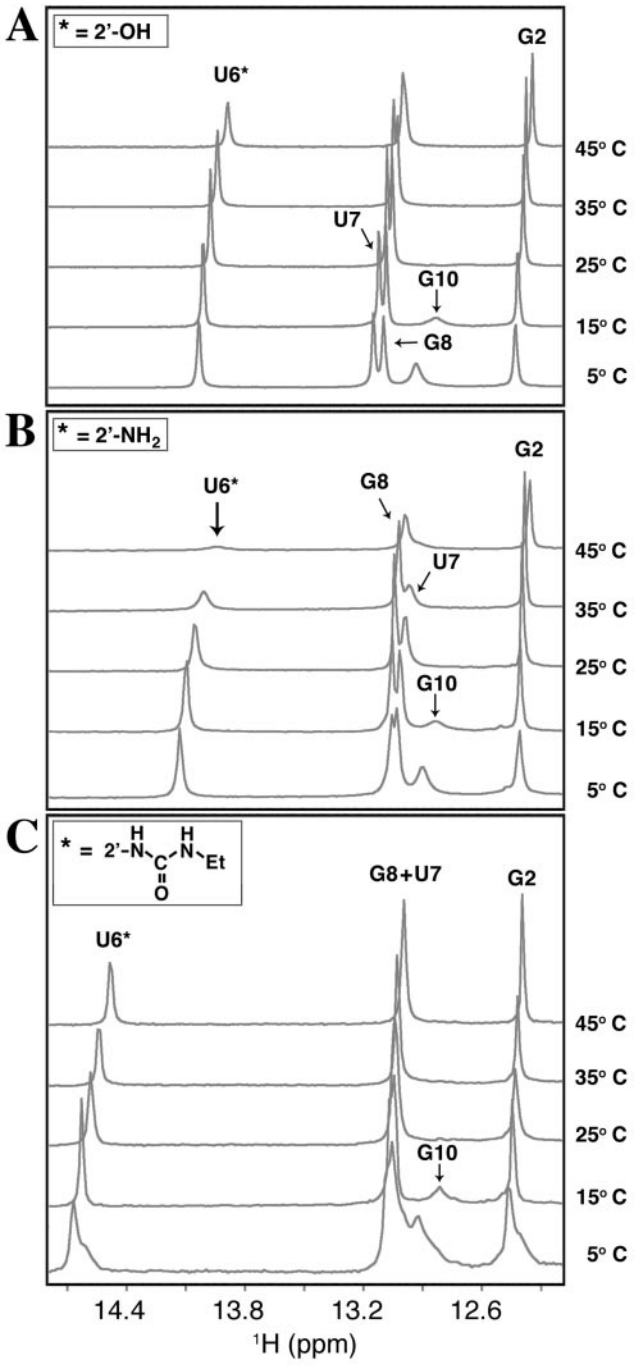

Figure 3. Imino region of 1D ^{1}H NMR spectra of 2′-modified RNAs at varying temperatures. (**A**) The stacked 1D ^{1}H NMR spectra of a modified, self-complementary duplex RNA (identical to the one shown in Figure 2B) collected at the temperatures shown on the right. The asterisk refers to the C2′ substituent on the U6 residue, which is a hydroxyl. The identities of the imino proton resonances are shown above the peaks or with arrows. (**B** and **C**) As in (A), but the C2′ substituents denoted with asterisks are amino (B) and ethylureido (C). All spectra were collected in 90% H_2O/10% D_2O.

The sample spectrum shown in Figure 4B demonstrates that the 2′-ethyl group is in close proximity to the H1′ protons of U6 and U7 residues. The terminal methyl protons of this group also show a strong NOE cross peak to the H2 proton of A5, which is the Watson–Crick pairing partner of U6 (data not shown). H1′ and H2 protons are situated on the surface of

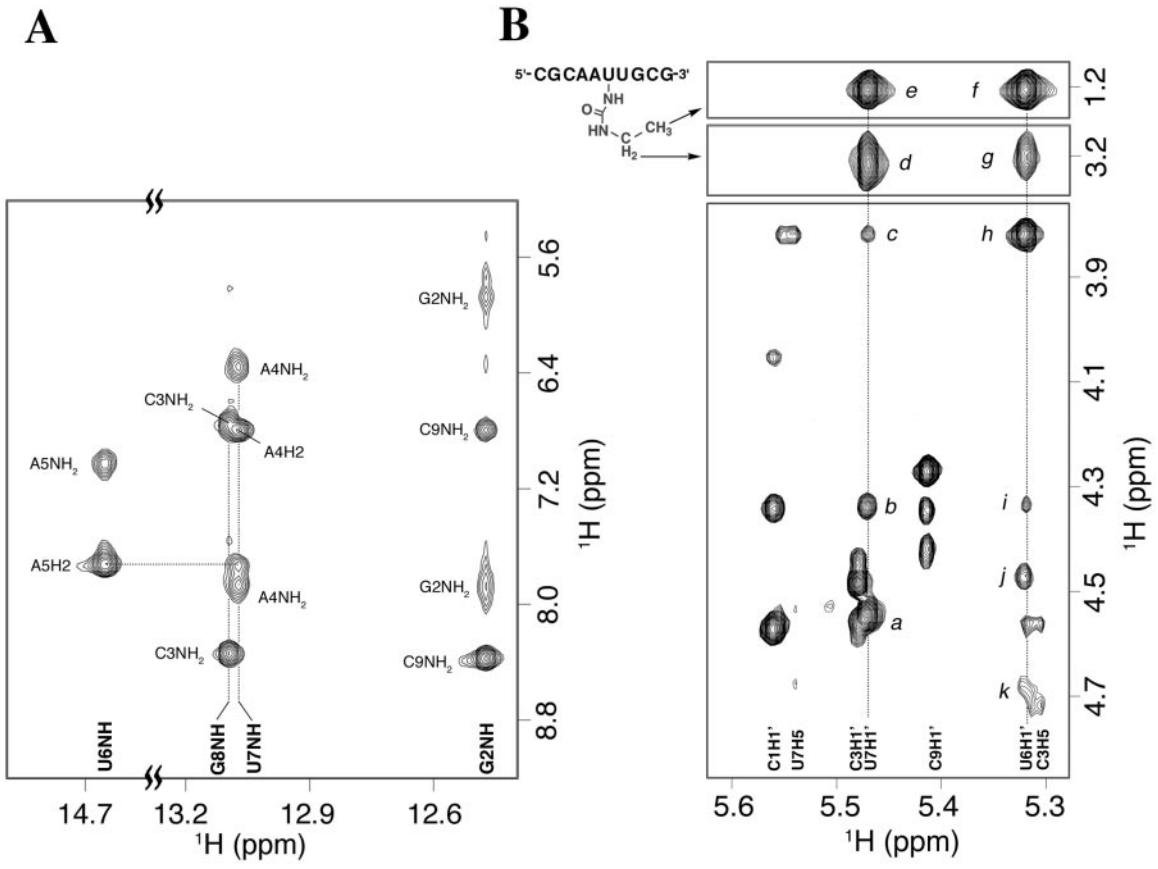

Figure 4. Sample 2D NOESY spectra of 2′-ethylureido-modified RNA in H_2O and D_2O. (**A**) The imino region of the 2D NOESY spectrum in H_2O. The sequence of the duplex RNA used was identical to the one used in Figures 2 and 3. Imino proton resonances are shown at the bottom and protons that exhibit NOEs with imino protons are denoted next to each cross peak. (**B**) Sample spectrum of the 2D NOESY in D_2O. H1′ protons of U6 and U7 form cross peaks with methyl and methylene protons of the C2′ substituent, which are denoted with arrows. The identities of all protons interacting with U6 and U7 H1′ protons are labeled a–k. They are as follows: a, U7H3′; b, U7H2′; c, U6H2′; d, U6HCG′; e, U6HCD′; f, U6HCG′; g, U6HCD′; h, U2H2′; i, A5H2′; j, U6H4′; and k, U6H3′.

the minor groove, indicating that the 2′-ethylureido group may be oriented inward, rather than sampling the available conformational space away from the RNA helix. To examine the orientation of the 2′-ethylureido group more quantitatively, we performed NMR-based molecular modeling experiments. All 10 models generated by CNS (25) in these experiments correlate well with one another based on the modeling statistics (Table 1). The models show that the 2′-ethylureido group lies on the surface of the minor groove (Figure 5A). The C2′ substituents do not sterically interfere with one another in the minor groove since there is no overlap between them in the space-filled rendering (Figure 5B). Furthermore, the ethyl groups are oriented towards opposite ends of the helix, directed away from one another (Figure 5B).

Upon closer inspection, the NB′ proton of the 2′-ureido group (the proton that is absent from the analogous 2′-amidonucleoside) is within hydrogen bonding distance with the O2 atom of the parent U6 base (Figure 5C). The presence of other NOEs is consistent with the interaction. For example, the NB′ proton also shows a strong NOE to the U6H2′ proton that is situated toward the interior of the minor groove, in close proximity to the O2 atom of U6 (Figure 5C). The apparent

Table 1. NMR-based modeling statistics

	2′-OH	2′-NH_2	2′-ethylureido
Restraint statistics			
NOE	112	104	130
Dihedral	130	130	134
H-bond	26	26	26
Restraint violations			
NOE (>0.5 Å)			
4–7 bp	0	0	0
Overall	2	1	0
Dihedral angle (>5°)			
4–7 bp	0	0	2[a]
overall	2	0	3.5
Average RMSDs from mean (Å)			
4–7 bp	0.25	0.25	0.19

Data from 2D NOESY experiments were used for subsequent structure modeling calculations. A total of 10 models were calculated for each RNA. The central 4 bp of all 10 models were superimposed and the pairwise atomic RMSD calculated.

[a]Dihedral angle violations (<13°) in the urea group of the 2′ substituent were deviations from the presumed planarity of the group. Literature evidence indicates that the minimum-energy structure of urea actually deviates from planarity, with out-of-plane hydrogen torsion angles of ∼13° and 150° (39).

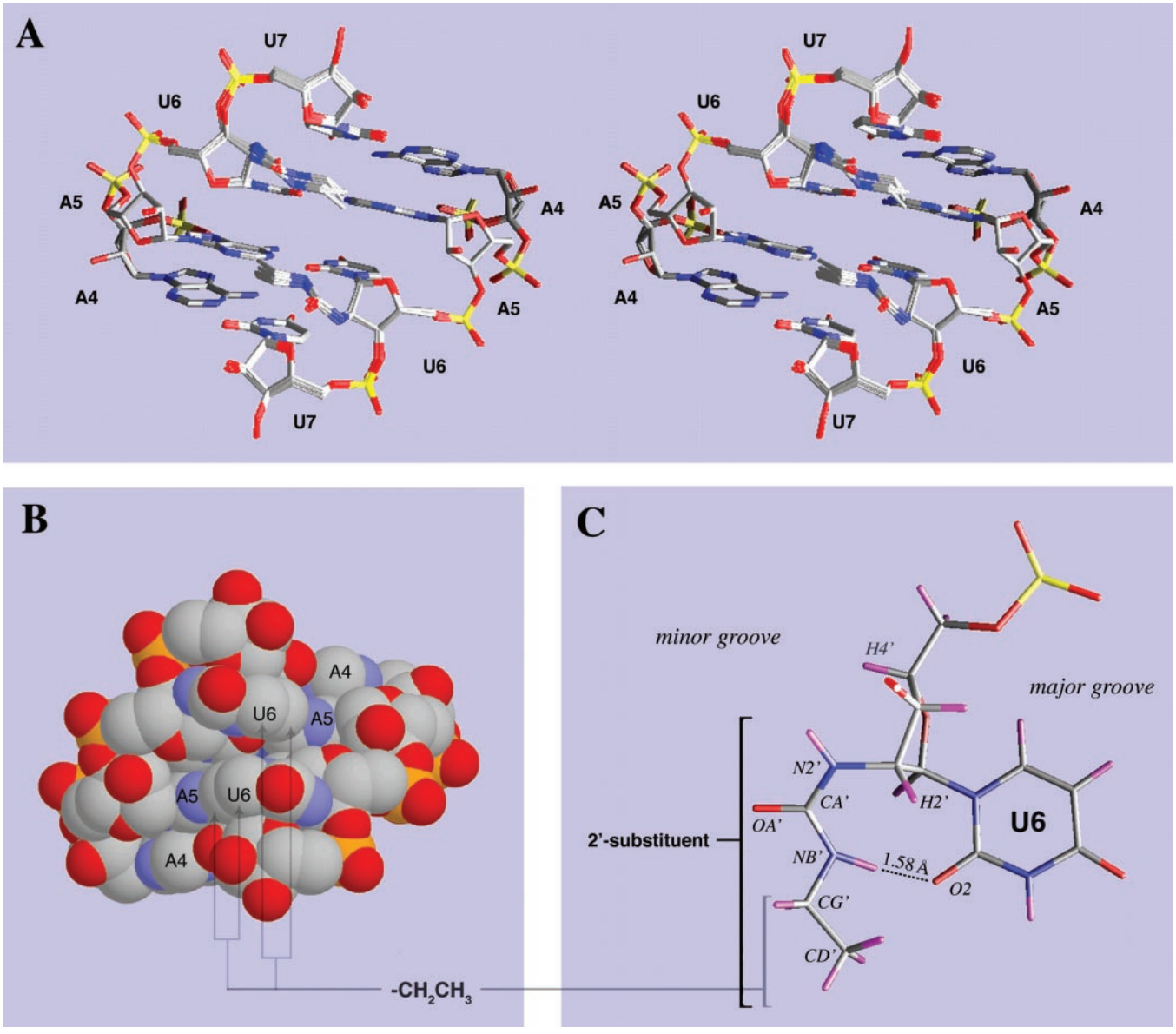

Figure 5. Structural models of 2′-ethylureido-modified RNA. (**A**) Stereoview of 10 superimposed structural models of 2′-ethylureido-modified RNA. Only the central four bases indicated in boldface (5′-CGC**AAUU**GCG-3′) are depicted. The minor groove side of the helix is shown. (**B**) Space-filled rendering of a representative model. The residues are identified on the image. Arrows point to the carbon atoms of the ethyl group of the C2′ substituent. (**C**) Isolated and enlarged view of the modified U6 residue, looking down the helix axis. The minor and major grooves are indicated to provide orientation. Selected atoms and the entire C2′ substituent are labeled. The dotted line indicates a hydrogen-bonding interaction.

hydrogen bonding interaction between HNB′ and O2 of U6 explains why the 2′-ureido group appears confined in the minor groove and may shed light on the increased stability of the 2′-ureido RNA relative to the other 2′-modified RNAs that we have examined. This hydrogen bonding interaction is also likely to occur in the 2′-ureido-modified cytidines since they have an identically positioned O2 atom. 2′-ureido-modified purines might also form a similar interaction since purine N3 atoms are analogously positioned to accept a hydrogen bond.

The data sets collected for the 2′-amino and 2′-hydroxyl RNAs were very similar to one another. With the exception of the H2′ and H3′ resonances of the modified U6 residue, there were no significant differences in chemical shift (Supplemental Table). Furthermore, the 2′-amino-modified U6 residue did not have significant C2′-*endo* character as determined by DQF-COSY and TOCSY experiments (data not shown). Since free 2′-aminouridine is known to adopt predominantly C2′-*endo* conformation (13), the RNA duplex may be forcing the 2′-amino-modified U6 residue into C3′-*endo* configuration. This is not surprising since RNAs are significantly more rigid than DNAs (32,33), which readily adopt C3′-*endo* conformation when modified with 2′-*O*-substituents (34). However, the RNA helix may adjust its conformation to accommodate the altered sugar pucker. This change could negatively affect helix stability.

DISCUSSION

We have characterized a series of 2′-nitrogen-modified RNA duplexes and have examined how the modifications affect RNA stability. The structural models we have generated for some of these RNAs provide a framework for understanding the effect of C2′ modifications on duplex stability.

All three of the 2′-nitrogen-modified RNAs we examined were less stable than unmodified RNA. Of these three RNAs, the 2′-ureido-modified one was the most stable. Our results are consistent with those of Sigurdsson and Eckstein, who demonstrated that an RNA duplex modified on one strand with a 2′-alkylureido group is more stable than an analogous 2′-amino-modified duplex (35). Based on our thermodynamic analysis, the increased thermal stability of the 2′-ureido-modified RNA is predominantly an enthalpic effect. The addition of the 2′-ureido group only results in a modest loss of favorable enthalpy compared with native 2′-hydroxyl RNA. In contrast, both 2′-amino- and 2′-amido-modified RNAs pay larger enthalpic penalties. Biala and Strazewski (36) have shown that differences in folding enthalpy are dominated by changes in RNA hydration. It is plausible that the increased stability of the 2′-ureido-modified RNA is strongly influenced by the hydration properties of the minor groove.

The 2′-ureido differs from the 2′-amido substituent only by an additional –NH– group. Our molecular modeling data suggest that this –NH– group can form an intra-residue hydrogen bonding interaction with the O2 atom of the uracil base. There may be an entropic penalty for this interaction. However, this interaction may also serve to stabilize 2′-ureido-modified RNAs. By restricting the mobility of the 2′-ureido group, the hydrogen bonding interaction may prevent unfavorable steric clashes with other RNA constituents. It may also affect interactions between water molecules and the RNA.

Egli *et al*. (32) have shown that water molecules extensively hydrate the minor groove. Their high-resolution crystal structure of duplex RNA shows that these water molecules form clusters, positioned around the phosphate backbone, O4′ and O2′. The waters that are localized near the 2′-OH group are of particular significance because, in addition to their interactions with the 2′-oxygen, they form secondary contacts that order the water structure in the minor groove. One of these water molecules forms an intra-residue bridge between the ribose O2′ and the pyrimidine O2. This water molecule, in turn, hydrogen bonds to another water molecule that mediates an identical interaction (between O2′ and O2) on the opposite strand of the RNA duplex. This type of interaction can also occur with purine N3 atoms in place of pyrimidine O2s. As a result, there is a network of water molecules, anchored by the 2′-OH, that traverses the minor groove and stabilizes the helix.

Our results indicate that the 2′-ureido group mimics this interaction, bridging the C2′ substituent and O2 as water molecules normally do in native RNA. In addition to restoring the bridging interaction, the ureido group may provide a hydrophilic surface for restoring the transverse water network. This interpretation is consistent with our thermodynamic data. The ordered water molecules should increase RNA hydration in the minor groove, contributing favorably to the enthalpy of duplex formation. The increased order would reduce the entropy of the system when compared to the other modified RNAs, as we observe. Although our data support this interpretation, high-resolution structural studies will be needed to confirm this model.

Unlike 2′-ureido-modified RNA, the 2′-amido-modified RNA cannot form the bridging interaction since it lacks a suitable hydrogen-bond donor. Because of this, the minor groove water network is almost certainly disrupted–if not by the lack of bonding partners, then by steric interference with the C2′ substituent. Again, our thermodynamic data are consistent with this interpretation.

The destabilization caused by the 2′-amino substitution is more difficult to explain in terms of hydration since the amino group is capable, in principle, of accepting a hydrogen bond from water and unlikely to perturb water molecules by steric interference. In fact, the water network may be intact. However, sugar puckering may not be the sole factor governing the stability of the 2′-amino-modified RNA since DNAs with similar modifications are also destabilized, despite being predisposed to C2′-*endo* configuration (15,16). It is possible that 2′-amino substitutions disrupt DNA in a distinct, unrelated way. But based on the existing data, we can only postulate that the 2′-aminonucleoside affects the overall stability of an RNA helix by adopting a C3′-*endo* conformation.

Our studies have helped us to understand better how C2′-modified RNAs affect helix stability. Importantly, they have aided us in our goal of developing a system for specific, rapid and reversible RNA cross-linking. Based on the structural models generated for the 2′-ureido-modified RNA, we initially placed the 2′-substituents in a sub-optimal structural context. In all our experiments, the C2′ modifications were placed on opposite strands of a double-helix, separated by 1 bp in the 5′ direction (relative to the top strand of the duplex, Figure 1B). However, our models indicate that, in this context, the functional groups will be oriented away from one another. Because the ureido group forms a specific interaction with the uridine base, we predict that other substituents attached to pyrimidine nucleosides via 2′-ureido linkages will adopt a similar configuration. Therefore, for cross-linking or for other applications where the 2′-ureido-linked substituents must be in close proximity to one another in the minor groove, it may be beneficial to place 2′-modifications on nucleosides separated in the 3′ direction (relative to the top strand, Figure 1B) or on Watson–Crick pairing partners. These structural contexts will increase the likelihood that the C2′ substituents will form the desired interactions in the minor groove. We note, however, that disulfide cross links can form using duplexes with 2′-ureido-linked alkylthiol modifications separated in the 5′ direction (23). This can be explained in two ways: (i) a subpopulation of the C2′ substituents may adopt an alternative conformation in solution or (ii) all the C2′ substituents may spend some fraction of their time in solution sampling conformational space. Disulfide cross-linking between modified nucleotides separated in the 5′ direction is quantitative (23), strengthening the latter explanation. However, the ability to form cross links in this structural context is not universal. Our preliminary cross-linking experiments with 2′-dithiol-modified duplexes indicate that the 2′-substituents must be separated in the 3′ direction, not in the 5′ direction, in order to bind an exogenous crosslinker (J.W.Pham and E.J.Sontheimer, unpublished data).

For applications that require an A-form helical background, 2′-ureido-linkages provide a superior alternative to 2′-amido ones. RNAs modified with these linkages can be prepared at near quantitative yields using an established method and, in a

helical context, are significantly more stable than analogous 2′-amido-modified RNAs. For applications that do not require a helical background, 2′-amido-linked modifications remain a viable option. These modifications are easily achieved using well-characterized chemistry. Furthermore, they do not require the use of isocyanates (used to form ureido linkages), which are relatively unstable compounds that are prone to hydrolysis.

SUPPLEMENTARY MATERIAL

Supplementary Material is available at NAR Online.

ACKNOWLEDGEMENTS

We thank Joshua Veatch and Roger Wu for their assistance with organic synthesis, Kai Huang and Ben Ramirez for their help in setting up NMR experiments, and Scott Silverman and Philip Bevilacqua for their helpful suggestions on melting analysis. NMR spectra of RNA samples were recorded in the WCAS Structural Biology NMR facility. Small molecule NMR and MALDI-TOF MS were performed in the Analytical Services Lab. Melting analysis was done in the Keck Biophysics Facility at Northwestern University. J.W.P. is a Presidential Fellow of Northwestern University and was supported by an NIH Biophysics Training Grant. This work was supported by a National Science Foundation CAREER Award to E.J.S.

REFERENCES

1. Leirdal,M. and Sioud,M. (1998) High cleavage activity and stability of hammerhead ribozymes with a uniform 2′-amino pyrimidine modification. *Biochem. Biophys. Res. Commun.*, **250**, 171–174.
2. Hendrix,C., Mahieu,M., Anne,J., Van Calenbergh,S., Van Aerschot,A., Content,J. and Herdewijn,P. (1995) Catalytic activity and stability of hammerhead ribozymes containing 2′-acetamido-2′-deoxyribonucleosides. *Biochem. Biophys. Res. Commun.*, **210**, 67–73.
3. Heidenreich,O., Benseler,F., Fahrenholz,A. and Eckstein,F. (1994) High activity and stability of hammerhead ribozymes containing 2′-modified pyrimidine nucleosides and phosphorothioates. *J. Biol. Chem.*, **269**, 2131–2138.
4. Herschlag,D., Eckstein,F. and Cech,T.R. (1993) The importance of being ribose at the cleavage site in the Tetrahymena ribozyme reaction. *Biochemistry*, **32**, 8312–8321.
5. Herschlag,D., Eckstein,F. and Cech,T.R. (1993) Contributions of 2′-hydroxyl groups of the RNA substrate to binding and catalysis by the Tetrahymena ribozyme. An energetic picture of an active site composed of RNA. *Biochemistry*, **32**, 8299–8311.
6. Fromme,J.C., Banerjee,A., Huang,S.J. and Verdine,G.L. (2004) Structural basis for removal of adenine mispaired with 8-oxoguanine by MutY adenine DNA glycosylase. *Nature*, **427**, 652–656.
7. Kent,O.A. and MacMillan,A.M. (2002) Early organization of pre-mRNA during spliceosome assembly. *Nature Struct. Biol.*, **9**, 576–581.
8. Sontheimer,E.J., Sun,S. and Piccirilli,J.A. (1997) Metal ion catalysis during splicing of premessenger RNA. *Nature*, **388**, 801–805.
9. Yean,S.L., Wuenschell,G., Termini,J. and Lin,R.J. (2000) Metal-ion coordination by U6 small nuclear RNA contributes to catalysis in the spliceosome. *Nature*, **408**, 881–884.
10. Iribarren,A.M., Sproat,B.S., Neuner,P., Sulston,I., Ryder,U. and Lamond,A.I. (1990) 2′-*O*-alkyl oligoribonucleotides as antisense probes. *Proc. Natl Acad. Sci. USA*, **87**, 7747–7751.
11. Prakash,T.P., Kawasaki,A.M., Lesnik,E.A., Owens,S.R. and Manoharan,M. (2003) 2′-*O*-[2-(amino)-2-oxoethyl] oligonucleotides. *Org. Lett.*, **5**, 403–406.
12. Cummins,L.L., Owens,S.R., Risen,L.M., Lesnik,E.A., Freier,S.M., McGee,D., Guinosso,C.J. and Cook,P.D. (1995) Characterization of fully 2′-modified oligoribonucleotide hetero- and homoduplex hybridization and nuclease sensitivity. *Nucleic Acids Res.*, **23**, 2019–2024.
13. Guschlbauer,W. and Jankowski,K. (1980) Nucleoside conformation is determined by the electronegativity of the sugar substituent. *Nucleic Acids Res.*, **8**, 1421–1433.
14. Uesugi,S., Miki,H., Ikehara,M., Iwahashi,H. and Kyogoku,Y. (1979) Linear relationship between electronegativity of 2′-substituents and conformation of adenine nucleosides. *Tetrahedron Lett.*, **42**, 4073–4076.
15. Hendrix,C., Devreese,B., Rozenski,J., van Aerschot,A., De Bruyn,A., Van Beeumen,J. and Herdewijn,P. (1995) Incorporation of 2′-amido-nucleosides in oligodeoxynucleotides and oligoribonucleotides as a model for 2′-linked conjugates. *Nucleic Acids Res.*, **23**, 51–57.
16. Aurup,H., Tuschl,T., Benseler,F., Ludwig,J. and Eckstein,F. (1994) Oligonucleotide duplexes containing 2′-amino-2′-deoxycytidines: thermal stability and chemical reactivity. *Nucleic Acids Res.*, **22**, 20–24.
17. Griffin,B.A., Adams,S.R. and Tsien,R.Y. (1998) Specific covalent labeling of recombinant protein molecules inside live cells. *Science*, **281**, 269–272.
18. Adams,S.R., Campbell,R.E., Gross,L.A., Martin,B.R., Walkup,G.K., Yao,Y., Llopis,J. and Tsien,R.Y. (2002) New biarsenical ligands and tetracysteine motifs for protein labeling *in vitro* and *in vivo*: synthesis and biological applications. *J. Am. Chem. Soc.*, **124**, 6063–6076.
19. Singh,R. and Whitesides,G.M. (1990) Comparisons of rate constants for thiolate-disulfide interchange in water and in polar aprotic-solvents using dynamic ^{1}H-NMR line-shape analysis. *J. Am. Chem. Soc.*, **112**, 1190–1197.
20. Kojima,M. (1970) Synthesis of 2-amino-1,2-propanedithiol and related compounds. *Yakugaku Zasshi*, **90**, 670–674.
21. Thalen,A. and Claeson,G. (1965) The preparation of 4-amino-1, 2-dithiolane and a discussion of its ultra-violet spectrum. *Arkiv Kemi*, **24**, 463–470.
22. Sigurdsson,S.T., Seeger,B., Kutzke,U. and Eckstein,F. (1996) A mild and simple method for the preparation of isocyanates from aliphatic amines using trichloromethyl chloroformate. Synthesis of an isocyanate containing an activated disulfide. *J. Org. Chem.*, **61**, 3883–3884.
23. Alefelder,S. and Sigurdsson,S.T. (2000) Interstrand disulfide cross-linking of internal sugar residues in duplex RNA. *Bioorg. Med. Chem.*, **8**, 269–273.
24. Marky,L.A. and Breslauer,K.J. (1987) Calculating thermodynamic data for transitions of any molecularity from equilibrium melting curves. *Biopolymers*, **26**, 1601–1620.
25. Brunger,A.T., Adams,P.D., Clore,G.M., DeLano,W.L., Gros,P., Grosse-Kunstleve,R.W., Jiang,J.S., Kuszewski,J., Nilges,M., Pannu,N.S. *et al.* (1998) Crystallography & NMR system: a new software suite for macromolecular structure determination. *Acta Crystallogr. D Biol. Crystallogr.*, **54**, 905–921.
26. Tidor,B., Irikura,K.K., Brooks,B.R. and Karplus,M. (1983) Dynamics of DNA oligomers. *J. Biomol. Struct. Dyn.*, **1**, 231–252.
27. Omichinski,J.G., Pedone,P.V., Felsenfeld,G., Gronenborn,A.M. and Clore,G.M. (1997) The solution structure of a specific GAGA factor–DNA complex reveals a modular binding mode. *Nature Struct. Biol.*, **4**, 122–132.
28. Nicholls,A., Sharp,K.A. and Honig,B. (1991) Protein folding and association: insights from the interfacial and thermodynamic properties of hydrocarbons. *Proteins*, **11**, 281–296.
29. Sayle,R.A. and Milner-White,E.J. (1995) RASMOL: biomolecular graphics for all. *Trends Biochem. Sci.*, **20**, 374.
30. Sigurdsson,S.T., Tuschl,T. and Eckstein,F. (1995) Probing RNA tertiary structure: interhelical crosslinking of the hammerhead ribozyme. *RNA*, **1**, 575–583.
31. Cohen,S. and Cech,T.R. (1997) Dynamics of thermal motions within a large catalytic RNA investigated by cross-linking with thiol-disulfide interchange. *J. Am. Chem. Soc.*, **119**, 6259–6268.
32. Egli,M., Portmann,S. and Usman,N. (1996) RNA hydration: a detailed look. *Biochemistry*, **35**, 8489–8494.
33. Venkateswarlu,D., Lind,K.E., Mohan,V., Manoharan,M. and Ferguson,D.M. (1999) Structural properties of DNA:RNA duplexes

containing 2′-*O*-methyl and 2′-*S*-methyl substitutions: a molecular dynamics investigation. *Nucleic Acids Res*., **27**, 2189–2195.
34. Lesnik,E.A., Guinosso,C.J., Kawasaki,A.M., Sasmor,H., Zounes,M., Cummins,L.L., Ecker,D.J., Cook,P.D. and Freier,S.M. (1993) Oligodeoxynucleotides containing 2′-*O*-modified adenosine: synthesis and effects on stability of DNA:RNA duplexes. *Biochemistry*, **32**, 7832–7838.
35. Sigurdsson,S.T. and Eckstein,F. (1996) Site specific labelling of sugar residues in oligoribonucleotides: reactions of aliphatic isocyanates with 2′-amino groups. *Nucleic Acids Res*., **24**, 3129–3133.
36. Biala,E. and Strazewski,P. (2002) Internally mismatched RNA: pH and solvent dependence of the thermal unfolding of tRNA(Ala) acceptor stem microhairpins. *J. Am. Chem. Soc*., **124**, 3540–3545.
37. Allawi,H.T. and SantaLucia,J.,Jr (1997) Thermodynamics and NMR of internal G·T mismatches in DNA. *Biochemistry*, **36**, 10581–10594.
38. SantaLucia,J.,Jr, Kierzek,R. and Turner,D.H. (1992) Context dependence of hydrogen bond free energy revealed by substitutions in an RNA hairpin. *Science*, **256**, 217–219.
39. Meier,R.J. and Coussens,B. (1992) The molecular structure of the urea molecule: is the minimum energy structure planar? *J. Mol. Struct*., **253**, 25–33.